

Facial Reenactment Through a Personalized Generator

ARIEL ELAZARY, Tel-Aviv University, Israel
 YOTAM NITZAN, Tel-Aviv University, Israel
 DANIEL COHEN-OR, Tel-Aviv University, Israel

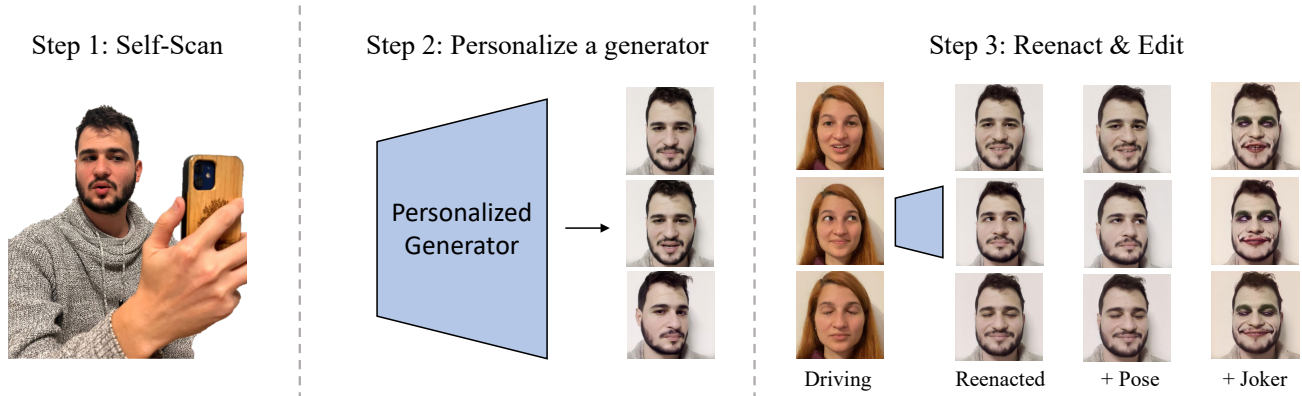


Fig. 1. We present a novel approach to reenact an individual using only a casual *self-scan*. Using a captured self-scan (Step 1), we train a personalized image generator, tailored specifically to that individual (Step 2). The personalized generator guarantees the preservation of the individual’s appearance and facilitates video-driven reenactment. Thanks to the generator’s semantic latent space, the generated video can be edited and stylized in post-process (Step 3).

In recent years, the role of image generative models in facial reenactment has been steadily increasing. Such models are usually subject-agnostic and trained on domain-wide datasets. The appearance of the reenacted individual is learned from a single image, and hence, the entire breadth of the individual’s appearance is not entirely captured, leading these methods to resort to unfaithful hallucination. Thanks to recent advancements, it is now possible to train a personalized generative model tailored specifically to a given individual. In this paper, we propose a novel method for facial reenactment using a personalized generator. We train the generator using frames from a short, yet varied, self-scan video captured using a simple commodity camera. Images synthesized by the personalized generator are guaranteed to preserve identity. The premise of our work is that the task of reenactment is thus reduced to accurately mimicking head poses and expressions. To this end, we locate the desired frames in the latent space of the personalized generator using carefully designed latent optimization. Through extensive evaluation, we demonstrate state-of-the-art performance for facial reenactment. Furthermore, we show that since our reenactment takes place in a semantic latent space, it can be semantically edited and stylized in post-processing.

CCS Concepts: • **Computing methodologies** → **Image manipulation**.

Additional Key Words and Phrases: Personalization, Facial Reenactment.

Authors’ addresses: Ariel Elazary, Tel-Aviv University, Israel; Yotam Nitzan, Tel-Aviv University, Israel; Daniel Cohen-Or, Tel-Aviv University, Israel.

Permission to make digital or hard copies of all or part of this work for personal or classroom use is granted without fee provided that copies are not made or distributed for profit or commercial advantage and that copies bear this notice and the full citation on the first page. Copyrights for components of this work owned by others than ACM must be honored. Abstracting with credit is permitted. To copy otherwise, or republish, to post on servers or to redistribute to lists, requires prior specific permission and/or a fee. Request permissions from permissions@acm.org.

© 2023 Association for Computing Machinery.

0730-0301/2023/7-ART \$15.00

<https://doi.org/10.1145/nnnnnnn.nnnnnnn>

ACM Reference Format:

Ariel Elazary, Yotam Nitzan, and Daniel Cohen-Or. 2023. Facial Reenactment Through a Personalized Generator. *ACM Trans. Graph.* 1, 1 (July 2023), 11 pages. <https://doi.org/10.1145/nnnnnnn.nnnnnnn>

1 INTRODUCTION

Facial reenactment is the task of synthesizing a realistic portrait video of a target person that replicates the actions of a person appearing in a driving video. The ability to do so is essential for movie postproduction, augmented reality (AR), virtual reality (VR) and telepresence applications. The main challenge of this task is faithfully representing the identity, or appearance, of the target person, in varying conditions.

For years, works approaching this task took a graphics perspective, explicitly modeling 3D geometry, usually relying on morphable mesh models [Grassal et al. 2022; Hu et al. 2017; Ichim et al. 2015; Kim et al. 2018; Lombardi et al. 2018; Thies et al. 2019, 2016; Zheng et al. 2022a]. Recently, several works have leveraged 2D image generative models for the task [Abdal et al. 2022; Lin et al. 2022; Sun et al. 2022; Wang et al. 2021b; Zakharov et al. 2019]. These methods offer superior image quality than those based on traditional 3D graphics as they inherently support more facial components including hair, the mouth cavity, and accessories like glasses. Moreover, a notable advantage of using generative models is that they support intuitive semantic control, such as aging or adding glasses, through their latent spaces [Abdal et al. 2020; Patashnik et al. 2021; Shen et al. 2020] and out-of-domain stylization [Gal et al. 2021; Ojha et al. 2021; Zhu et al. 2021] (see Fig. 1).

Although methods relying on image generative models have many advantages, they compromise identity preservation. Previous works have primarily used one or just a few images (e.g., 8) to learn the appearance of the target person [Abdal et al. 2022; Lin et al. 2022;

Sun et al. 2022; Wang et al. 2021b]. Using one or very few images is usually claimed as an advantage as they are easy to obtain. However, the full variance and aspects of a person’s appearance clearly cannot be learned in this setting. To complete missing information, such methods resort to hallucination based on generic face priors learned from many different individuals. Realistically, beyond data acquisition, another factor popularizing this setting was the lack of methods to train a generator to preserve identity as portrayed in a reasonably sized personal photo album.

In this work, we leverage recent advancements in generative modelling and employ an *image generator* that is *personalized* – *i.e.* trained specifically for a given person. As input, we take a *self-scan* – a short RGB video that captures the target person in a variety of viewpoints and facial expressions. Such a self-scan video, albeit short, is sufficient to personalize a domain-wide (*i.e.*, faces) image generator [Karras et al. 2020] and enables a faithful modelling of the person’s identity. Importantly, the self-scan is still easy to obtain as it is casually captured using any standard camera and does not require a high-cost apparatus nor a controlled environment nor a strict script to follow.

To personalize the generative model, we build upon MyStyle [Nitzan et al. 2022]. Requiring roughly 100 – 300 images of an individual, MyStyle fine-tunes a generic face generator [Karras et al. 2020] to model the individual’s identity. Importantly, other properties of the generator, such as the image quality and semantic latent space are preserved. Using the personalized generator immediately mitigates the challenge of preserving identity. Reenactment is then reduced to locating a code in the generator’s latent space that imitates the head pose and expression of the person in a driving frame, which we perform using *latent optimization*.

This optimization is nevertheless challenging in itself. Common representations for pose and expression are often entangled with the identity information. For example, facial keypoints [Kartynnik et al. 2019] are often used to track facial motion and specifically used to indicate on the person’s pose and expression. However, keypoints also indicate the facial geometry and were shown to encode identity [Nixon 1985]. Due to this fact, previous works leveraging keypoints were limited to only have a person reenacting themselves (*i.e.*, *self-reenactment*) [Zakharov et al. 2019]. We overcome this difficulty by using a keypoint-driven representation from which we eliminate most identity-related information. Concisely, we use a carefully selected subset of keypoints and represent each with a relative location, with respect only to other keypoints belonging to the same facial part (*e.g.*, left eye). To capture additional information that is overlooked by the keypoints, such as the presence of teeth, we directly use the driving frame’s pixels in specific regions. We optimize the latent code to according to these two terms. Note that neither term is perfectly agnostic to identity, which might hinder identity preservation if used in a different setting. However, the personalized generator is constrained to identity-preserving results and the optimization can only recover the nearest possible solution.

A key challenge in video generation is maintaining temporal consistency. Although two consecutive frames are similar, two separate optimization processes might converge to latent codes that are unnecessarily different. To mitigate temporal inconsistency, we initialize each optimization process with a slightly noised version of

the latent code produced for the previous frame. Since optimization is highly susceptible to its initialization, this approach biases the optimization to converge to a nearby latent and hence, minimizes unnecessary perturbation between the two consecutive frames.

Through quantitative and qualitative evaluation, we demonstrate that our method is highly effective at facial reenactment. Specifically, we find that our method excels at identity preservation, surpassing the performance of recent state-of-the-art methods, and performs at least on par in terms of transferring pose and expression.

2 RELATED WORK

2.1 Facial Reenactment

Facial Reenactment was traditionally approached from a 3D-graphics perspective. Such methods usually start by collecting significant footage of the target face and reconstructing an explicit 3D mesh model, using 3D Morphable Models [Blanz and Vetter 1999]. At test time, reenactment is performed by transferring pose and expression from the 3D model of the driving video to that of the target 3D face model [Blanz et al. 2003; Bouaziz et al. 2013; Cao et al. 2014, 2013; Garrido et al. 2014; Grassal et al. 2022; Hu et al. 2017; Ichim et al. 2015; Thies et al. 2015, 2016]. A thorough introduction of facial reconstruction and 3DMM is provided in recent surveys [Egger et al. 2020; Zollhöfer et al. 2018]. Explicitly modeling faces in 3D is challenging and most methods struggle with modelling hair, mouth cavity and accessories like glasses.

Recently, different approaches were proposed to sidestep these challenges. First, several works avoided 3D modelling altogether by warping an image of the target face [Averbuch-Elor et al. 2017; Drobyshev et al. 2022; Siarohin et al. 2019]. With this approach, faithful changes to pose and expression possible are relatively limited, often leading to undesired artifacts. A second approach models faces using other 3D representations such as neural implicit representations [Gafni et al. 2021; Zheng et al. 2022a] and point clouds [Zheng et al. 2022b]. Last, and most relevant to our work, several recent works have incorporated 2D generative models, mostly GANs [Goodfellow et al. 2014], to their pipelines. Some of these works have proposed pipelines that are entirely identity-agnostic. *I.e.*, a generative model is trained on a domain-wide dataset, and a single image of the individual is used as a starting point for manipulation [Abdal et al. 2022; Hong et al. 2022; Lin et al. 2022; Sun et al. 2022; Wang et al. 2021b, 2022].

A single image is insufficient to learn the entire breadth of appearances of an individual, leading such methods to resort to unfaithful hallucination. Accordingly, other works have incorporated more footage of the individual on top of generic knowledge of faces. Kim et al. [2018] and the concurrent work by Wang et al. [2023] classically perform reenactment using 3DMM but employ person-specific generative models to transform 3DMM-based renders to realistic images. Inevitably, they still partially suffer from limitations stemming from using 3D mesh models, such as not modeling the mouth cavity. A different approach, also taken by this work, is pretraining the model on a domain-wide dataset and then fine-tuning it for a specific individual. Zakharov et al. [2019] pretrain on VoxCeleb [Chung et al. 2018], a low-resolution ($\leq 256p$) video dataset, limiting the eventual quality of their output. Their method is also limited to only support

an individual reenacting themselves. Cao et al. [2022] pretrain on an unpublished dataset that is laborious to collect, featuring hundreds of identities, performing scripted facial expressions while being captured by 90 cameras simultaneously. In contrast, our domain-wide model is an off-the-shelf StyleGAN2 [Karras et al. 2020] model, trained on FFHQ [Karras et al. 2019] – a high-resolution (1024p) image dataset, that is crawled off the Internet. Our simple pretraining approach is significantly more accessible, does not compromise output quality, and could naturally be improved by using future image datasets.

2.2 Generative Prior

In recent years, generative models have immensely improved in countless foundational tasks such as unconditional synthesis [Brock et al. 2018; Karras et al. 2019], image-to-image translation [Isola et al. 2017; Zhu et al. 2017] and text-condition synthesis [Ramesh et al. 2022; Rombach et al. 2022]. Noticeably, unconditional GANs [Goodfellow et al. 2014], and specifically StyleGAN [Karras et al. 2019, 2020], have drawn attention for the meaningful representations that emerge in the generator’s latent space. Such meaningful representations make the generator useful for numerous downstream applications, beyond simply image synthesis. One line of works find semantic controls in the generator’s latent space which enable controlled synthesis and image editing pipelines [Abdal et al. 2020; Härkönen et al. 2020; Patashnik et al. 2021; Shen et al. 2020; Shen and Zhou 2020; Voynov and Babenko 2020]. Other works leverage these pretrained generators as a prior for downstream tasks ranging from image enhancement [Chan et al. 2021; Gu et al. 2020; Luo et al. 2020; Menon et al. 2020; Pan et al. 2021; Richardson et al. 2021; Wang et al. 2021a; Yang et al. 2021], facial reenactment [Abdal et al. 2022; Lin et al. 2022; Nitzan et al. 2020; Sun et al. 2022] and even discriminative tasks, such as regression [Xu et al. 2021].

Methods leveraging unconditional GANs often start with locating a latent code that corresponds to a desired image. This process, often known as *projection*, can be carried out using a trained encoder [Nitzan et al. 2020; Pidhorskyi et al. 2020; Richardson et al. 2021; Tov et al. 2021; Xu et al. 2021] or using optimization [Abdal et al. 2019; Gu et al. 2020; Karras et al. 2020; Parmar et al. 2022; Zhu et al. 2020]. Encoding is significantly faster than optimization, but is also less accurate.

Regardless of the projection method, the desired image might not exist within the output space of the generator, greatly limiting the applicability of this approach. To overcome this challenge, several works have proposed to slightly fine-tune the generator in order to improve its expressiveness on specific inputs [Bau et al. 2020; Nitzan et al. 2022; Pan et al. 2021; Roich et al. 2021]. Within this line of works, Nitzan et al. [2022] recently proposed MyStyle – a method to fine-tune the generator to faithfully model a specific person.

In this work, we rely on MyStyle’s personalized generator as prior for reenactment. Technically, we locate the desired frame by projecting aspects of the driving frame such as facial keypoints and the eyes and mouth regions.

3 METHOD

We aim to generate a portrait video in which a target person, appearing in a self-scan video, is repeating the actions occurring in a

driving video. The self-scan is a short, yet varied, RGB video used to learn the appearance of the target individual. The simple process of capturing a self-scan is discussed in subsection 3.1. Our approach is composed of two steps. First, using the self-scan, we train a personalized image generator, building upon MyStyle [Nitzan et al. 2022] (subsection 3.2). The personalized generator is a universal representation of the individual, and can be used in conjunction to any driving video. Second, we perform latent optimization to locate a latent code of the personalized generator that faithfully represents the actions in a driving frame (subsection 3.3).

3.1 Self-Scan Capture

To authentically model an individual’s appearance, one must observe them in a wide variety of settings. For example, the best, or perhaps only, way of knowing how a person looks like when smiling is to actually see them smiling beforehand.

We find that a short, single-take, RGB video can include sufficiently varied head poses and expressions. We call such videos *self-scans*, as they can be conveniently captured by the individual themselves. Note that the individual does not need to be following any script. Instead, the self-scan should intuitively include the poses and expressions that one desires to be possible for the generated video. One does not need to exhaust all combinations of poses and expressions, and performing each once is sufficient. As we demonstrate later, our method enables disentangling and recomposing poses and expressions that were not seen jointly in the self-scan.

In practice, for the experiments in this paper, we instructed several individuals to capture a 20-30 seconds, portrait video of themselves with varying head poses and expressions that could be used in a social interaction, like conversation.

3.2 From a Self-Scan to a Personalized Generator

At the core of our method is an unconditional personalized generator G , mapping a latent code to an image. To train it, we employ the recently proposed method MyStyle [Nitzan et al. 2022]. Using an image dataset of an individual, MyStyle slightly fine-tunes StyleGAN2 [Karras et al. 2020], a generic face image generator, to obtain a generator that faithfully preserves individual’s appearance.

Creating the Training Set. StyleGAN2 and MyStyle are trained on aligned portrait images. We therefore start with *smoothly* aligning and cropping all frames in the self-scan [Tzaban et al. 2022].

MyStyle was demonstrated effective when used with a dataset of 100-300 randomly curated images. A self-scan, however, is composed of significantly more frames, often over a thousand. Increasing the training set size slows training and inference times, due to increased dimensionality [Nitzan et al. 2022]. We observe that not all frames are required for training. Many frames are similar to each other – consecutive frames, for example, are nearly duplicates. Using two frames that are interchangeable adds negligible diversity and information to the generator. Intuitively, one of these frames could be omitted.

Let us denote the set of aligned self-scan crops by S . We wish to find a subset $T \subset S$, where T contains a predetermined number of frames, marked N , and maximizes the subset’s “diversity”. Following previous works [Nitzan et al. 2022; Ojha et al. 2021], we use the

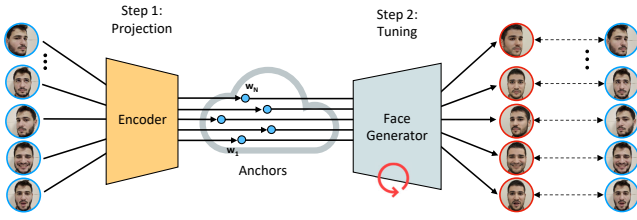


Fig. 2. An illustration of MyStyle’s tuning method. A set of N portrait images of the target individual are projected into StyleGAN’s latent space. The result is a set of anchors that are the nearest possible neighbors. We then tune the generator to reconstruct the input images from their corresponding anchors according to Eq. (1).

average pairwise LPIPS [Zhang et al. 2018] distances as a measure of a set’s diversity. Identifying the optimal subset T is known to be NP-hard but a greedy algorithm was proven to be quite effective [Ravi et al. 1994]. The greedy algorithm iteratively adds the element of the set $S \setminus T$ whose minimal distance to any element of current subset T is greatest. See pseudo-code description in Algorithm 1 in the supplemental. We find that $N = 250$ is sufficient.

MyStyle training. Using the filtered self-scan we next train MyStyle [Nitzan et al. 2022]. Due to MyStyle’s central role in training and later on in reenactment, we concisely repeat the training details.

We start with our training set $T = \{t_i\}_{i=1}^N$ and a StyleGAN2 generator [Karras et al. 2020] pretrained on FFHQ [Karras et al. 2019]. Each image t_i is first inverted into StyleGAN’s latent space \mathcal{W} , yielding a latent code w_i , called *anchor*. Inversion is performed using an off-the-shelf inversion encoder, whose architecture follows Richardson et al. [2021]. Now, the pretrained StyleGAN2 generator is fine-tuned using pivotal tuning [Roich et al. 2021] – *i.e.*, to better reconstruct the training images from their corresponding anchors. Formally, the training loss is given by

$$\mathcal{L}_{\text{mystyle}} = \sum_{i=1}^N [\mathcal{L}_{\text{lpips}}(G(w_i), t_i) + \lambda_{\text{pixel}} \|G(w_i) - t_i\|_2], \quad (1)$$

where $\mathcal{L}_{\text{lpips}}$ is the LPIPS loss [Zhang et al. 2018] and $\lambda_{\text{pixel}} = 10$ is a hyperparameter balancing the two terms.

We illustrate the training process in Fig. 2.

3.3 Reenactment by Latent Optimization

Identity preservation, the paramount challenge of reenactment, is guaranteed from using the personalized generator G . Therefore, the task is reduced to accurately reproducing head poses and facial expressions of the driving frames. To this end, we employ *latent optimization* on each driving frame, directly optimizing a latent code such that the image generated from it would be suitable. An overview of the process is illustrated in Fig. 4.

3.3.1 Latent Space. MyStyle’s point-wise training (Eq. (1)) affects only certain regions of the latent space, making them preserve the individual’s identity [Nitzan et al. 2022]. These regions are modeled well by a slightly dilated convex hull defined by the anchors $\{w_i\}_{i=1}^N$. To ensure identity preservation, Nitzan et al. [2022] used the convex hull as the generator’s latent space, instead of the latent spaces

commonly used with StyleGAN, such as \mathcal{W} and \mathcal{W}^+ [Abdal et al. 2019]. We similarly adopt and make use of the personalized subspace, dubbed \mathcal{P}^+ , for latent optimization. A thorough and formal introduction of the latent space is provided in Appendix B.

3.3.2 Loss Function. To guide optimization towards a latent code that replicates the desired head pose and facial expression, we use 3D facial keypoints. Some aspects of expression, like the mouth cavity, are overlooked by keypoints. Therefore, we also employ a pixel-reconstruction loss directly in specific regions, as will be soon discussed.

Keypoints Loss. Indicating the locations and shapes of facial parts, facial keypoints hold rich information regarding head pose and facial expression. However, keypoints are also affected by the unique appearance of each individual [Nixon 1985]. Therefore, forcing a target identity to replicate keypoints of another individual leads to unsatisfactory results, and restricted previous works to only support self-reenactment [Zakharov et al. 2019]. We propose an alternative guidance, derived from keypoints, that similarly indicates pose and expression but is significantly more robust to identity.

Specifically, we start from a set of 468 3D keypoints estimated using off-the-shelf method, MediaPipe [Kartynnik et al. 2019], and make several modifications, illustrated in Fig. 3.

We first consider only a subset of all keypoints. Most keypoints are essential for modeling face geometry, but carry very little semantic meaning. Compare, for example, keypoints on the cheeks or forehead with those on the eyes and mouth. The eyes and mouth are perceptually more significant and receive special attention in keypoint estimation [Grishchenko et al. 2020] and reenactment [Zakharov et al. 2019]. Even within the mouth, keypoints indicating whether the mouth is open or closed are crucial, but those that indicate the shape of the lips are person-specific and thus irrelevant. Accordingly, we use a subset of keypoints that constitutes only of – inner parts of both lips, eyelids and irises.

One can still deduce the distances between the eyes and mouth from our subset of keypoints. This information is again person-specific and was even used directly in early face recognition methods [Nixon 1985]. We overcome this problem by separately normalizing keypoints of the *same* facial part to have zero mean. Since all keypoints are now relative, they cannot be used to deduce pose. We therefore bring back four individual keypoints, indicating the frame of the head, which are used with their original absolute image coordinates. In total, we use 66 keypoints – 16 for each eye, 5 for each iris, 20 for the mouth and 4 for the frame of the head.

Finally, the keypoint-based loss function is the sum of distances between keypoints of the driving and generated images. Formally,

$$\mathcal{L}_{\text{key}} = \sum_{i=1}^{66} \|\text{keypoints}(I_d)_i - \text{keypoints}(I_g)_i\|_2, \quad (2)$$

where $\text{keypoints}()$ is the operation extracting our subset of keypoints from the driving and generated images I_d, I_g , respectively.

Pixel Losses. Facial keypoints do not model some aspects of expression, most notably – the mouth cavity, and solely relying on them hinders the fidelity of results [Kim et al. 2018; Wang et al. 2023; Zakharov et al. 2019; Zheng et al. 2022a]. For example, even with a

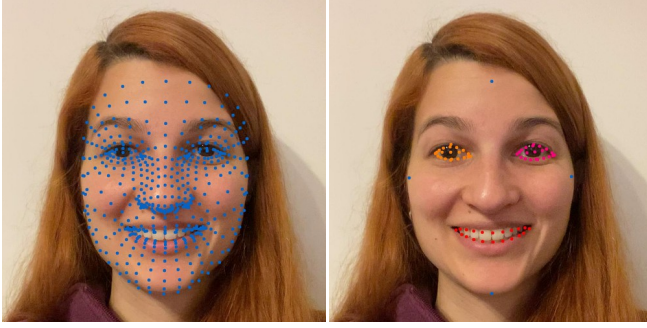


Fig. 3. Comparison of all keypoints inferred by MediaPipe [Kartynnik et al. 2019] (left) with our reduced subset (right). The subset chosen conveys pose and expression while being significantly less sensitive to identity. Colors other than blue indicate the grouping according to facial parts. The keypoints of each facial part are normalized separately to have zero mean. The blue landmarks are used with their absolute, non-normalized, coordinates.

perfectly transferred lips motion, teeth might inappropriately appear or disappear from generated frames. To mitigate this issue, we impose a loss that encourages actual pixel reconstruction between the mouth region of the driving and generated frames. Formally, this loss reads as

$$\mathcal{L}_{\text{mouth}} = \|\text{mouth}(I_d) - \text{mouth}(I_g)\|_2, \quad (3)$$

where *mouth* is the operation of cropping and resizing the mouth region, as defined by keypoints, from the driving and generated images I_d, I_g (see Appendix C for details).

At first, this loss might appear counter-productive as it encourages copying regions from the driving individual to the target individual – harming identity preservation. However, this is not a concern in our case, since using a personalized generator guarantees identity preservation. The added pixel loss can only guide the optimization towards the “nearest” possible solution, which is necessarily identity preserving.

We find that another region that requires special attention is that of the irises. Aiming for an expressive reenactment setting, the irises should be able to convey any expression, such as looking right or down. However, StyleGAN perpetuates biases inherited from FFHQ, where irises are almost always looking towards the camera. We find the personalized generator is able to reconstruct the “iris expressions” seen in the self-scan but struggles to generalize beyond them.

In practice, the keypoint-driven optimization is able to reproduce the iris at the right location, at the price of its color – often producing an off-white iris. We find it possible to recover the correct eye color by adding a dedicated pixel reconstruction loss on the irises. Formally, the loss reads as

$$\mathcal{L}_{\text{eyes}} = \|\text{left-eye}(I_c) - \text{left-eye}(I_g)\|_2 + \|\text{right-eye}(I_c) - \text{right-eye}(I_g)\|_2, \quad (4)$$

where *left-eye* and *right-eye* are the operations of cropping and resizing these regions from (details in Appendix C) the generated image I_g and an image serving as reference for the identity I_c . The

reference image I_c is generated from the center of the personalized subspace.

Overall Loss. The overall reenactment loss reads as

$$\mathcal{L}_{\text{full}} = \mathcal{L}_{\text{key}} + \lambda_{\text{mouth}} \mathcal{L}_{\text{mouth}} + \lambda_{\text{eyes}} \mathcal{L}_{\text{eyes}} + \lambda_{\text{reg}} \mathcal{L}_{\text{reg}}, \quad (5)$$

where \mathcal{L}_{reg} is a regularization term adopted from MyStyle that is partially responsible for optimization being constrained to the latent space \mathcal{P}^+ , and is thoroughly explained in Appendix B.

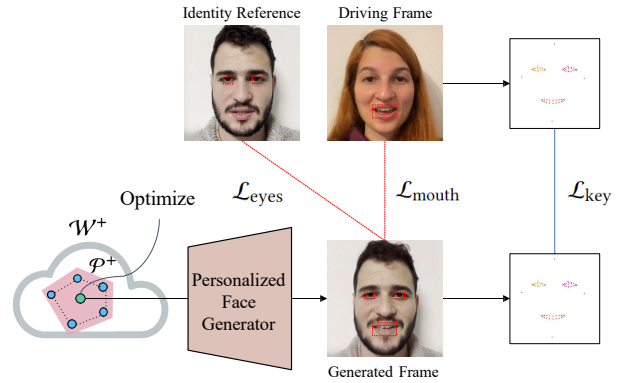


Fig. 4. Illustration of our latent optimization method for generating a reenacted frame. We operate within the personalized latent space \mathcal{P}^+ of the generator, ensuring identity preservation and reducing the task to reproducing pose and expression. To this end, we employ three losses to compare the generated and driving frames. First, we penalize differences in a subset of keypoints [Kartynnik et al. 2019], which are separately normalized (indicated by color) for each facial part to have zero mean. The subset of normalized keypoints still conveys pose and expression but is more robust to geometry. Second, we apply an L_2 reconstruction loss on pixels in the mouth cavity between driving and generated frame for expression fidelity. Third, we apply an L_2 reconstruction loss on pixels in the irises areas between identity reference, which is generated from the center of \mathcal{P}^+ , and generated frame for color preservation.

3.3.3 Temporal Consistency. Operating on each frame individually oftentimes leads to temporally incoherent results. We follow the approach proposed by Tzaban et al. [2022], where temporal coherency is inherited from the input video by using smooth operations on individual frames. We take several independent steps.

Similar to the training set, driving frames must also be aligned. The crop and alignment performed are determined using facial keypoints [Karras et al. 2019], which we smooth with a Gaussian low-pass filter. Next, each optimization process is initialized with the result of the previous frame, with small additive Gaussian noise. Adding noise is necessary to allow optimization escape the local minima of using the previous latent code again. We find that this initialization is crucial for biasing the optimization to consistently converge to nearby latent codes, minimizing unnecessary perturbation. We finally apply another Gaussian low-pass filter, this time on the produced latent codes themselves, making the transition between frames even smoother.

Table 1. Comparison to competing methods, in terms of identity preservation (IDP), identity consistency (IDC), average expression distance (AED), average pose distance (APD), and NIQE [Mittal et al. 2012].

	ID(↑)	APD _{×100} (↓)	AED _{×10} (↓)	NIQE (↓)
NHA	0.80	0.24	2.37	19.34
LIA	0.71	0.13	1.59	45.52
DaGAN	0.73	0.26	1.77	34.88
Ours	0.89	0.16	1.52	13.22

4 EXPERIMENTS

In the following experiments we use 8 self-scans of individuals from various genders, ages and ethnicities. A sample of our results is displayed in Fig. 8, and additional videos are available in the supplemental. We start by comparing our method to state-of-the-art facial reenactment methods, qualitatively and quantitatively in subsection 4.1. In subsection 4.2, we demonstrate that by performing reenactment through a semantic latent space, we can intuitively apply semantic editing and stylization in post-process. We then evaluate the design choices of our method through an ablation study in subsection 4.3, and the generator’s ability to generalize beyond the pretraining data and even the self-scan data by novelty composing expressions in subsection 4.4.

4.1 Comparison

Baselines. We first compare our method with three state-of-the-art methods. We choose works representative of several of the main branches of facial reenactment literature, as described below. Neural Head Avatars (NHA) [Grassal et al. 2022] receives as input a single video and explicitly models 3D mesh surface. Reenactment is performed by transferring parameters between 3D morphable models [Li et al. 2017]. We note that NHA’s video is “professionally” taken – *i.e.* taken in front of a green screen, with even lighting, and is also $\times 3$ longer than ours. Latent Image Animator (LIA) [Wang et al. 2022] is a *one-shot* method, taking in a single image as input, and warping it to match driving frames. The warp is determined according to latent controls learned by a 2D generative model trained for that purpose. DaGAN [Hong et al. 2022] is a one-shot method, using a dedicated 2D image-to-image translation module, translating each driving frame to a reenactment frame.

Comparison Protocol. Here, we use 4 of our self-scans videos. We use each video separately as a self-scan, and also to drive the other self-scans. We use random 5-10 seconds sequences from the driving videos and produce a total of 10 results. We note that one-shot methods are given the first frontal-pose, neutral-expression frame in the video of the target individual, and video-based methods use entire video. NHA also requires an indication of one such frame.

We use multiple quantitative metrics to evaluate the performance of reenactment. First, We measure identity preservation (ID) with respect to the training set. To this end, we follow a protocol similar to MyStyle’s, where for each reenacted frame we compute its average similarity to the top-5 most similar images in the training set and average across all frames. We use top-5 images (instead of

MyStyle’s top-1), to prevent one-shot methods from being trivially similar to their reference image. Similarity is measured in terms of cosine similarity of features extracted from a face recognition network [Deng et al. 2019a].

Next, we measure pose and expression preservation from the driving video. Following previous works [Lin et al. 2022; Sun et al. 2022], we measure Average Pose Distance (APD) and Average Expression Distance (AED). Both are defined as the mean square error of deep features extracted by a 3D face reconstruction model [Deng et al. 2019b]. Last, we evaluate the frame’s quality. Due to the few-shot nature of the problem, popular metrics such as FID are unsuitable. We instead use NIQE [Mittal et al. 2012], a metric designed to evaluate image quality without reference.

We report the metrics in Tab. 1, a set of qualitative results in Fig. 9, and videos in the supplemental. As can be seen, our method outperform all existing methods on identity and expression preservation, and quality, and performs competitively with the leader LIA on pose preservation. Specifically, by comparing generated images to reference self-scan frames, one can observe that our method excels at preserving identity.

4.2 Edits and Stylization in Post-Process

Our reenactment method is built on top of an incredibly semantic image generator – StyleGAN. We can therefore leverage the myriad of applications and methods designed for StyleGAN, adding new capabilities on top of reenactment. In this section we demonstrate two such capabilities, performed in post-process – semantic editing and stylization. Results for both applications are presented in Fig. 5.

Semantic Editing. In StyleGAN’s latent space there exist vectors or “directions” that when traversed upon, affect the generated image in a semantically consistent manner. For example, one such vector would consistently and gradually add a smile. The result of our latent optimization method is a set of latent codes, that turn into the reenacted video once passed through the generator. Here, instead of generating frames from these latent codes, we first shift them a constant sized step in the direction of a specific semantic vector. Passing these shifted latent codes through the generator results in a reenacted video that was semantically additionally edited. We use three semantic vectors that are identified using InterFaceGAN [Shen et al. 2020] – smile, pose, and age.

Stylization. Several methods [Gal et al. 2021; Ojha et al. 2021] have been proposed to fine-tune StyleGAN slightly so that it models different data domains. These fine-tuned models are known to be *aligned* with their parent models, *i.e.* images generated by the two models, from the same latent code, correspond to each other [Wu et al. 2021]. Here, we further fine-tune our personalized models with StyleGAN-NADA [Gal et al. 2021], a text-driven training method. We fine-tune with two prompts – “the Joker” and “a sketch”. The latent optimization still takes place in the personalized generator, but the resulting latent codes are passed through the generator tuned with StyleGAN-NADA to produce the final video frames. The result is a reenacted video which depicts the target individual but they are stylized as the Joker or a sketch.



Fig. 6. Ablation study. Evenly spaced self-scan frames miss uncommon expressions, like closing eyes, prohibiting from reproducing them (e.g., first row). The naive keypoint-driven reenactment method does not generalize between different facial geometries and completely fails transferring expressions. Last, adding the pixel loss \mathcal{L}_{crop} , generally improves the expression preservation efficacy and specifically encourages accurate appearance of teeth in the mouth cavity.

As can be seen in Fig. 5, the reenacted frames are successfully edited and stylized. This native post-process capability greatly extends the potential applications of our method and further encourages the use of semantic generative models as backbones for reenactment.

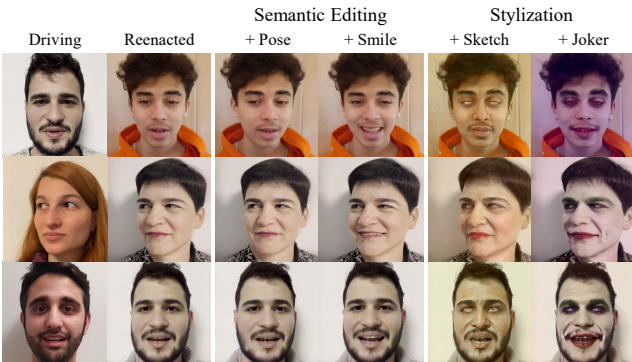


Fig. 5. Semantic editing and stylization of the reenacted video performed in post-process. Before being generated, the reenacted video is represented as a sequence of codes in StyleGAN’s latent space. The reenacted video can thus be semantically edited by shifting these latent codes in semantic directions [Shen et al. 2020] before feeding them to the generator, or stylized by feeding them to a generator that was fine-tuned for a specific style [Gal et al. 2021].

4.3 Ablation Studies

We next evaluate the contribution of individual aspects of our method through an ablation study. A sample of results is provided in Fig. 6.

The personalized generator is trained on a subset of self-scan frames that maximizes diversity. Here, we instead train personalized

models on frames that are evenly spaced across the self-scan, using the same number of frames $N = 250$. We find that these models fail to reproduce relatively uncommon expressions, such as closing the eyes. The reason becomes immediately clear when looking at the training set – these expressions, purely by chance, are entirely not present.

We move on to consider the latent optimization process. First, we use the naive optimization loss for keypoint-driven reenactment – penalizing differences in absolute keypoint coordinates. We find that all expressions are poorly reproduced. This is expected, since these keypoint representations are entangled with facial geometry and do not trivially correspond across individuals. Next, we reinstate our keypoint loss \mathcal{L}_{key} , but still without any pixel loss. While pose and expression are better preserved, differences from the driving frames are still clear, most notably in the shape of the lips and the appropriate appearance of teeth in the mouth cavity. Our final method, adding the pixel loss \mathcal{L}_{crop} immediately mitigates these issues.

4.4 Studying the Generator’s Expressiveness

Our reenactment through latent optimization could be considered a retrieval of the most suitable frame from the personalized generator. It is thus intriguing to ask – *what can and cannot it generate?* For this study, we use the relatively unusual expression of winking. Results are displayed in Fig. 7.

We first look at the generic StyleGAN model trained on FFHQ [Karras et al. 2019]. We apply our latent optimization method, using an inverted image [Roich et al. 2021] as initialization and a winking driving frame as guidance. This approach produces results that are not winking and are severely degraded.

We now capture a self-scan that is scripted to intentionally include a single instances of winking, with a neutral faces expression and frontal pose. From the self-scan we create two training set, where one is created normally and the from the other we omit the few winking frames. We train a personalized model with each of these training sets. Applying our reenactment method with winking driving frames to the two models, we find that only the model that has seen a wink in training is able to generate winking frames. We note that the generated winking frames are varied, composing a wink with other expressions and poses that were not seen in the single winking training instance.

We deduce two important conclusions. First, including unique expressions, and possibly other information, extends the model’s expressive power beyond what is provided by pre-training. On the flip side, an expression that is absent from the self-scan may not be produced. Second, the model can compose expressions and poses that were never seen together in training. This allows self-scans to be casually captured, not requiring a strict script and an exhaustive coverage of all setting combinations.

5 DISCUSSION AND CONCLUSION

Limitations. We have demonstrated that our method produces state-of-the-art results. Nevertheless, our method has a few limitations. First, as discussed in subsection 4.4 and Fig. 7, our generator is bounded by the variations appearing in the self-scan. Driving frames

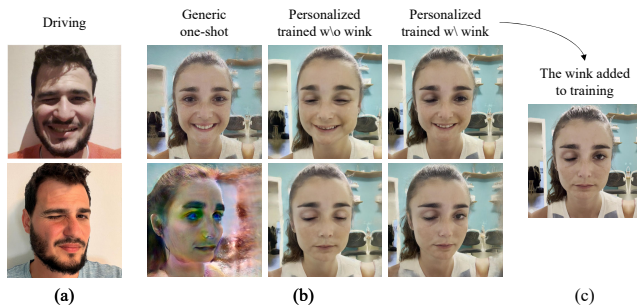


Fig. 7. Evaluating different generator’s ability to produce a wink. We reenact a target individual with two winking driving frames, seen in (a), through different models (b). The generic StyleGAN model, used in a one-shot manner, fails to produce winking faces and severely degrades the generated images in the process. A personalized model whose training set does not include a wink also fails to a wink. Nevertheless, the optimization being confined to the generator’s personalized subspace assures that the produced images are not degraded and faithfully preserve the individual’s appearance. Last, adding a single instance of winking (c) to the training set, allows the personalized generator to produce winking images. Note that the generated images compose a wink with a smile and a head pose that were not seen in training.

that depict unseen behavior, mostly expressions, would produce low fidelity results. Second, the optimization process performed per frame is time-consuming, requiring up to a minute for a single frame.

Conclusion. We have proposed a novel facial reenactment method leveraging a personalized image generator, trained on a casual self-scan of a single individual. Identity preservation is guaranteed by the generator being personalized, and thus we have reduced reenactment to reproducing poses and expressions, solved using a latent optimization process. Our experiments and analysis demonstrated that our method outperforms prior work in quality and fidelity, specifically excelling at identity preservation.

This study highlights the potential of 2D generative models for reenactment beyond the one/few-shot setting, effectively bridging a gap between the 2D and 3D streams of works. We hope it will inspire others to pursue this direction further. A natural first step would be to develop an encoder to replace latent optimization, substantially accelerating the process.

ACKNOWLEDGMENTS

We are grateful to Or Patashnik for insightful discussions throughout this work. We also thank Or Patashnik and Omer Tov for proofreading the draft. We finally thank Michal Elazary, Yogev Nitzan, Daniel Garibi, Zvia Elazary, Inbal Raz and Noa Rubin for providing us with their self-scans. This research was supported in part by the Israel Science Foundation (grants no. 2492/20 and 3441/21).

REFERENCES

Rameen Abdal, Yipeng Qin, and Peter Wonka. 2019. Image2stylegan: How to embed images into the StyleGAN latent space?. In *Proceedings of the IEEE international conference on computer vision*. 4432–4441.

Rameen Abdal, Peihao Zhu, Niloy Mitra, and Peter Wonka. 2020. StyleFlow: Attribute-conditioned Exploration of StyleGAN-Generated Images using Conditional Continuous Normalizing Flows. *arXiv preprint arXiv:2008.02401* (2020).

Rameen Abdal, Peihao Zhu, Niloy J Mitra, and Peter Wonka. 2022. Video2StyleGAN: Disentangling Local and Global Variations in a Video. *arXiv preprint arXiv:2205.13996* (2022).

Hadar Averbuch-Elor, Daniel Cohen-Or, Johannes Kopf, and Michael F Cohen. 2017. Bringing portraits to life. *ACM Transactions on Graphics (TOG)* 36, 6 (2017), 1–13.

David Bau, Hendrik Strobelt, William Peebles, Jonas Wulff, Bolei Zhou, Jun-Yan Zhu, and Antonio Torralba. 2020. Semantic photo manipulation with a generative image prior. *arXiv preprint arXiv:2005.07727* (2020).

Volker Blanz, Curzio Basso, Tomaso Poggio, and Thomas Vetter. 2003. Reanimating faces in images and video. In *Computer graphics forum*, Vol. 22. Wiley Online Library, 641–650.

Volker Blanz and Thomas Vetter. 1999. A morphable model for the synthesis of 3D faces. In *Proceedings of the 26th annual conference on Computer graphics and interactive techniques*. 187–194.

Sofien Bouaziz, Yangang Wang, and Mark Pauly. 2013. Online modeling for realtime facial animation. *ACM Transactions on Graphics (TOG)* 32, 4 (2013), 1–10.

Andrew Brock, Jeff Donahue, and Karen Simonyan. 2018. Large scale GAN training for high fidelity natural image synthesis. *arXiv preprint arXiv:1809.11096* (2018).

Chen Cao, Qiming Hou, and Kun Zhou. 2014. Displaced dynamic expression regression for real-time facial tracking and animation. *ACM Transactions on Graphics (TOG)* 33, 4 (2014), 1–10.

Chen Cao, Tomas Simon, Jin Kyu Kim, Gabe Schwartz, Michael Zollhofer, Shun-Suke Saito, Stephen Lombardi, Shih-En Wei, Danielle Belko, Shou-I Yu, et al. 2022. Authentic volumetric avatars from a phone scan. *ACM Transactions on Graphics (TOG)* 41, 4 (2022), 1–19.

Chen Cao, Yanlin Weng, Stephen Lin, and Kun Zhou. 2013. 3D shape regression for real-time facial animation. *ACM Transactions on Graphics (TOG)* 32, 4 (2013), 1–10.

Kelvin CK Chan, Xintao Wang, Xiangyu Xu, Jinwei Gu, and Chen Change Loy. 2021. Glean: Generative latent bank for large-factor image super-resolution. In *Proceedings of the IEEE/CVF Conference on Computer Vision and Pattern Recognition*. 14245–14254.

J. S. Chung, A. Nagrani, and A. Zisserman. 2018. VoxCeleb2: Deep Speaker Recognition. In *INTERSPEECH*.

Jiankang Deng, Jia Guo, Niannan Xue, and Stefanos Zafeiriou. 2019a. Arcface: Additive angular margin loss for deep face recognition. In *Proc. CVPR*. 4690–4699.

Yu Deng, Jialong Yang, Sicheng Xu, Dong Chen, Yunde Jia, and Xin Tong. 2019b. Accurate 3D Face Reconstruction with Weakly-Supervised Learning: From Single Image to Image Set. In *IEEE Computer Vision and Pattern Recognition Workshops*.

Nikita Drobyshev, Jency Chelishew, Taras Khakhulin, Aleksei Ivakhnenko, Victor Lempitsky, and Egor Zakharov. 2022. Megaportraits: One-shot megapixel neural head avatars. *arXiv preprint arXiv:2207.07621* (2022).

Bernhard Egger, William AP Smith, Ayush Tewari, Stefanie Wuhrer, Michael Zollhofer, Thabo Beeler, Florian Bernard, Timo Bolkart, Adam Kortylewski, Sami Romdhani, et al. 2020. 3d morphable face models—past, present, and future. *ACM Transactions on Graphics (TOG)* 39, 5 (2020), 1–38.

Michael S Floater. 2015. Generalized barycentric coordinates and applications. *Acta Numerica* 24 (2015), 161–214.

Guy Gafni, Justus Thies, Michael Zollhofer, and Matthias Nießner. 2021. Dynamic neural radiance fields for monocular 4d facial avatar reconstruction. In *Proceedings of the IEEE/CVF Conference on Computer Vision and Pattern Recognition*. 8649–8658.

Rimon Gal, Or Patashnik, Haggai Maron, Gal Chechik, and Daniel Cohen-Or. 2021. Stylegan-nada: Clip-guided domain adaptation of image generators. *arXiv preprint arXiv:2108.00946* (2021).

Pablo Garrido, Levi Valgaerts, Ole Rehmsen, Thorsten Thormahlen, Patrick Perez, and Christian Theobalt. 2014. Automatic face reenactment. In *Proceedings of the IEEE conference on computer vision and pattern recognition*. 4217–4224.

Ian Goodfellow, Jean Pouget-Abadie, Mehdi Mirza, Bing Xu, David Warde-Farley, Sherjil Ozair, Aaron Courville, and Yoshua Bengio. 2014. Generative adversarial nets. In *Advances in neural information processing systems*. 2672–2680.

Philip-William Grassal, Malte Prinzler, Titus Leistner, Carsten Rother, Matthias Nießner, and Justus Thies. 2022. Neural head avatars from monocular RGB videos. In *Proceedings of the IEEE/CVF Conference on Computer Vision and Pattern Recognition*. 18653–18664.

Ivan Grishchenko, Artsiom Ablavatski, Yuriy Kartynnik, Karthik Raveendran, and Matthias Grundmann. 2020. Attention mesh: High-fidelity face mesh prediction in real-time. *arXiv preprint arXiv:2006.10962* (2020).

Jinjin Gu, Yujun Shen, and Bolei Zhou. 2020. Image processing using multi-code gan prior. In *Proceedings of the IEEE/CVF conference on computer vision and pattern recognition*. 3012–3021.

Erik Härkönen, Aaron Hertzmann, Jaakko Lehtinen, and Sylvain Paris. 2020. Ganspace: Discovering interpretable gan controls. *Advances in Neural Information Processing Systems* 33 (2020), 9841–9850.

Fa-Ting Hong, Longhao Zhang, Li Shen, and Dan Xu. 2022. Depth-aware generative adversarial network for talking head video generation. In *Proceedings of the IEEE/CVF Conference on Computer Vision and Pattern Recognition*. 3397–3406.

Liwen Hu, Shunsuke Saito, Lingyu Wei, Koki Nagano, Jaewoo Seo, Jens Fursund, Iman Sadeghi, Carrie Sun, Yen-Chun Chen, and Hao Li. 2017. Avatar digitization from



Fig. 8. A sample of qualitative reenactment results produced by our method (center). Frames from the relevant self-scan are provided on both sides. Our method successfully reproduces poses and expression from the driving video while faithfully preserving the target identity. We recommend zooming in and carefully evaluating identity preservation by carefully comparing generated and self-scan frames.



Fig. 9. Comparing ours and state-of-the-art reenactment methods – NHA [Grassal et al. 2022], LIA [Wang et al. 2022] and DaGAN [Hong et al. 2022]. Frames from the self-scans of the target identity are provided on both sides. One-shot methods – LIA and DaGAN – take as input only the top image, marked with a black outline. As can be seen, our results are at least on par at transferring pose and expression and significantly better at realism and preserving identity. We recommend zooming in and carefully evaluating identity preservation by carefully comparing generated and self-scan frames.

a single image for real-time rendering. *ACM Transactions on Graphics (TOG)* 36, 6 (2017), 1–14.

Alexandru Eugen Ichim, Sofien Bouaziz, and Mark Pauly. 2015. Dynamic 3D avatar creation from hand-held video input. *ACM Transactions on Graphics (TOG)* 34, 4 (2015), 1–14.

Phillip Isola, Jun-Yan Zhu, Tinghui Zhou, and Alexei A Efros. 2017. Image-to-image translation with conditional adversarial networks. In *Proceedings of the IEEE conference on computer vision and pattern recognition*. 1125–1134.

Tero Karras, Samuli Laine, and Timo Aila. 2019. A style-based generator architecture for generative adversarial networks. In *Proc. CVPR*. 4401–4410.

Tero Karras, Samuli Laine, Miika Aittala, Janne Hellsten, Jaakko Lehtinen, and Timo Aila. 2020. Analyzing and improving the image quality of StyleGAN. In *Proc. CVPR*. 8110–8119.

Yury Kartynnik, Artsiom Ablavatski, Ivan Grishchenko, and Matthias Grundmann. 2019. Real-time facial surface geometry from monocular video on mobile GPUs. *arXiv preprint arXiv:1907.06724* (2019).

Hyeonwoo Kim, Pablo Garrido, Ayush Tewari, Weipeng Xu, Justus Thies, Matthias Niessner, Patrick Pérez, Christian Richardt, Michael Zollhöfer, and Christian Theobalt. 2018. Deep video portraits. *ACM Transactions on Graphics (TOG)* 37,

- 4 (2018), 1–14.
- Tianye Li, Timo Bolkart, Michael J Black, Hao Li, and Javier Romero. 2017. Learning a model of facial shape and expression from 4D scans. *ACM Trans. Graph.* 36, 6 (2017), 194–1.
- Connor Z Lin, David B Lindell, Eric R Chan, and Gordon Wetzstein. 2022. 3d gan inversion for controllable portrait image animation. *arXiv preprint arXiv:2203.13441* (2022).
- Stephen Lombardi, Jason Saragih, Tomas Simon, and Yaser Sheikh. 2018. Deep appearance models for face rendering. *ACM Transactions on Graphics (ToG)* 37, 4 (2018), 1–13.
- Xuan Luo, Xuaner Zhang, Paul Yoo, Ricardo Martin-Brualla, Jason Lawrence, and Steven M Seitz. 2020. Time-travel rephotography. *arXiv preprint arXiv:2012.12261* (2020).
- Sachit Menon, Alexandru Damian, Shijia Hu, Nikhil Ravi, and Cynthia Rudin. 2020. Pulse: Self-supervised photo upsampling via latent space exploration of generative models. In *Proceedings of the IEEE/CVF conference on computer vision and pattern recognition*. 2437–2445.
- Anish Mittal, Rajiv Soundararajan, and Alan C Bovik. 2012. Making a “completely blind” image quality analyzer. *IEEE Signal processing letters* 20, 3 (2012), 209–212.
- Yotam Nitzan, Kfir Aberman, Qiyu He, Orly Liba, Michal Yarom, Yossi Gandelsman, Inbar Mosseri, Yael Pritch, and Daniel Cohen-Or. 2022. Mystyle: A personalized generative prior. *ACM Transactions on Graphics (TOG)* 41, 6 (2022), 1–10.
- Yotam Nitzan, Amit Bermano, Yangyan Li, and Daniel Cohen-Or. 2020. Face Identity Disentanglement via Latent Space Mapping. *ACM Trans. Graph.* 39, 6, Article 225 (Nov. 2020), 14 pages. <https://doi.org/10.1145/3414685.3417826>
- Mark Nixon. 1985. Eye spacing measurement for facial recognition. In *Applications of digital image processing VIII*, Vol. 575. SPIE, 279–285.
- Utkarsh Ojha, Yijun Li, Jingwan Lu, Alexei A Efros, Yong Jae Lee, Eli Shechtman, and Richard Zhang. 2021. Few-shot Image Generation via Cross-domain Correspondence. *arXiv preprint arXiv:2104.06820* (2021).
- Xingang Pan, Xiaohang Zhan, Bo Dai, Dahua Lin, Chen Change Loy, and Ping Luo. 2021. Exploiting deep generative prior for versatile image restoration and manipulation. *IEEE Transactions on Pattern Analysis and Machine Intelligence* (2021).
- Gaurav Parmar, Yijun Li, Jingwan Lu, Richard Zhang, Jun-Yan Zhu, and Krishna Kumar Singh. 2022. Spatially-adaptive multilayer selection for gan inversion and editing. In *Proceedings of the IEEE/CVF Conference on Computer Vision and Pattern Recognition*. 11399–11409.
- Or Patashnik, Zongze Wu, Eli Shechtman, Daniel Cohen-Or, and Dani Lischinski. 2021. StyleCLIP: Text-Driven Manipulation of StyleGAN Imagery. *arXiv preprint arXiv:2103.17249* (2021).
- Stanislav Pidhorskyi, Donald A Adjeroh, and Gianfranco Doretto. 2020. Adversarial Latent Autoencoders. In *Proceedings of the IEEE/CVF Conference on Computer Vision and Pattern Recognition*. 14104–14113.
- Aditya Ramesh, Prafulla Dhariwal, Alex Nichol, Casey Chu, and Mark Chen. 2022. Hierarchical text-conditional image generation with clip latents. *arXiv preprint arXiv:2204.06125* (2022).
- Sekharipuram S Ravi, Daniel J Rosenkrantz, and Giri Kumar Tayi. 1994. Heuristic and special case algorithms for dispersion problems. *Operations Research* 42, 2 (1994), 299–310.
- Elad Richardson, Yuval Alaluf, Or Patashnik, Yotam Nitzan, Yaniv Azar, Stav Shapiro, and Daniel Cohen-Or. 2021. Encoding in style: a StyleGAN encoder for image-to-image translation. In *Proc. IEEE/CVF CVPR*. 2287–2296.
- Daniel Roich, Ron Mokady, Amit H Bermano, and Daniel Cohen-Or. 2021. Pivotal Tuning for Latent-based Editing of Real Images. *arXiv preprint arXiv:2106.05744* (2021).
- Robin Rombach, Andreas Blattmann, Dominik Lorenz, Patrick Esser, and Björn Ommer. 2022. High-resolution image synthesis with latent diffusion models. In *Proceedings of the IEEE/CVF Conference on Computer Vision and Pattern Recognition*. 10684–10695.
- Yujun Shen, Ceyuan Yang, Xiaoou Tang, and Bolei Zhou. 2020. InterFaceGAN: Interpreting the Disentangled Face Representation Learned by GANs. *arXiv preprint arXiv:2005.09635* (2020).
- Yujun Shen and Bolei Zhou. 2020. Closed-Form Factorization of Latent Semantics in GANs. *arXiv preprint arXiv:2007.06600* (2020).
- Aliaksandr Siarohin, Stéphane Lathuilière, Sergey Tulyakov, Elisa Ricci, and Nicu Sebe. 2019. First order motion model for image animation. *Advances in Neural Information Processing Systems* 32 (2019).
- Jingxiang Sun, Xuan Wang, Lizhen Wang, Xiaoyu Li, Yong Zhang, Hongwen Zhang, and Yebin Liu. 2022. Next3D: Generative Neural Texture Rasterization for 3D-Aware Head Avatars. *arXiv preprint arXiv:2211.11208* (2022).
- Justus Thies, Michael Zollhöfer, and Matthias Nießner. 2019. Deferred neural rendering: Image synthesis using neural textures. *ACM Transactions on Graphics (TOG)* 38, 4 (2019), 1–12.
- Justus Thies, Michael Zollhöfer, Matthias Nießner, Levi Valgaerts, Marc Stamminger, and Christian Theobalt. 2015. Real-time expression transfer for facial reenactment. *ACM Trans. Graph.* 34, 6 (2015), 183–1.
- Justus Thies, Michael Zollhöfer, Marc Stamminger, Christian Theobalt, and Matthias Nießner. 2016. Face2face: Real-time face capture and reenactment of rgb videos. In *Proceedings of the IEEE conference on computer vision and pattern recognition*. 2387–2395.
- Omer Tov, Yuval Alaluf, Yotam Nitzan, Or Patashnik, and Daniel Cohen-Or. 2021. Designing an Encoder for StyleGAN Image Manipulation. *arXiv preprint arXiv:2102.02766* (2021).
- Rotem Tzaban, Ron Mokady, Rinon Gal, Amit Bermano, and Daniel Cohen-Or. 2022. Stitch it in time: Gan-based facial editing of real videos. In *SIGGRAPH Asia 2022 Conference Papers*. 1–9.
- Andrey Voynov and Artem Babenko. 2020. Unsupervised Discovery of Interpretable Directions in the GAN Latent Space. *arXiv preprint arXiv:2002.03754* (2020).
- Lizhen Wang, Xiaochen Zhao, Jingxiang Sun, Yuxiang Zhang, Hongwen Zhang, Tao Yu, and Yebin Liu. 2023. StyleAvatar: Real-time Photo-realistic Portrait Avatar from a Single Video. *arXiv preprint arXiv:2305.00942* (2023).
- Ting-Chun Wang, Arun Mallya, and Ming-Yu Liu. 2021b. One-shot free-view neural talking-head synthesis for video conferencing. In *Proceedings of the IEEE/CVF conference on computer vision and pattern recognition*. 10039–10049.
- Xintao Wang, Yu Li, Honglun Zhang, and Ying Shan. 2021a. Towards Real-World Blind Face Restoration with Generative Facial Prior. In *Proceedings of the IEEE/CVF Conference on Computer Vision and Pattern Recognition*. 9168–9178.
- Yaohui Wang, Di Yang, Francois Bremond, and Antitza Dantcheva. 2022. Latent image animator: Learning to animate images via latent space navigation. *arXiv preprint arXiv:2203.09043* (2022).
- Zongze Wu, Yotam Nitzan, Eli Shechtman, and Dani Lischinski. 2021. StyleAlign: Analysis and Applications of Aligned StyleGAN Models. *arXiv preprint arXiv:2110.11323* (2021).
- Yinghao Xu, Yujun Shen, Jiapeng Zhu, Ceyuan Yang, and Bolei Zhou. 2021. Generative Hierarchical Features from Synthesizing Images. In *CVPR*.
- Tao Yang, Peiran Ren, Xuansong Xie, and Lei Zhang. 2021. GAN Prior Embedded Network for Blind Face Restoration in the Wild. In *Proceedings of the IEEE/CVF Conference on Computer Vision and Pattern Recognition*. 672–681.
- Egor Zakharov, Aliaksandra Shysheya, Egor Burkov, and Victor Lempitsky. 2019. Few-shot adversarial learning of realistic neural talking head models. In *Proceedings of the IEEE/CVF international conference on computer vision*. 9459–9468.
- Richard Zhang, Phillip Isola, Alexei A Efros, Eli Shechtman, and Oliver Wang. 2018. The unreasonable effectiveness of deep features as a perceptual metric. In *Proceedings of the IEEE conference on computer vision and pattern recognition*. 586–595.
- Yufeng Zheng, Victoria Fernández Abrevaya, Marcel C Böhler, Xu Chen, Michael J Black, and Otmar Hilliges. 2022a. Im avatar: Implicit morphable head avatars from videos. In *Proceedings of the IEEE/CVF Conference on Computer Vision and Pattern Recognition*. 13545–13555.
- Yufeng Zheng, Wang Yifan, Gordon Wetzstein, Michael J. Black, and Otmar Hilliges. 2022b. PointAvatar: Deformable Point-based Head Avatars from Videos.
- Jiapeng Zhu, Yujun Shen, Deli Zhao, and Bolei Zhou. 2020. In-domain GAN inversion for real image editing. *arXiv preprint arXiv:2004.00049* (2020).
- Jun-Yan Zhu, Taesung Park, Phillip Isola, and Alexei A Efros. 2017. Unpaired image-to-image translation using cycle-consistent adversarial networks. In *Proc. IEEE ICCV*. 2223–2232.
- Peihao Zhu, Rameen Abdal, John Femiani, and Peter Wonka. 2021. Mind the gap: Domain gap control for single shot domain adaptation for generative adversarial networks. *arXiv preprint arXiv:2110.08398* (2021).
- Michael Zollhöfer, Justus Thies, Pablo Garrido, Derek Bradley, Thabo Beeler, Patrick Pérez, Marc Stamminger, Matthias Nießner, and Christian Theobalt. 2018. State of the art on monocular 3D face reconstruction, tracking, and applications. In *Computer graphics forum*, Vol. 37. Wiley Online Library, 523–550.

A SUPPLEMENTAL OVERVIEW

In Appendix B we elaborate on details related to the latent optimization process that were kept out of the main paper in sake of clarity. Then, Appendix C provides technical implementation details.

B LATENT SPACE FOR OPTIMIZATION

At the core of our method is a latent optimization process in the latent space of a personalized generator, trained with MyStyle [Nitzan et al. 2022]. To ensure identity preservation, MyStyle use a novel latent space for all its downstream application. In this work, we adopt this latent space, without any modifications. This section thoroughly describes how we use that latent space, partially repeating discussions appearing in MyStyle for the sake of completeness.

B.1 Native Latent Space, \mathcal{P}

Nitzan et al. [2022] observed that only a certain region of the generator’s latent space has been personalized as result of training (see subsection 3.2). To capture this region, they propose using a slightly “dilated” convex hull spanned by the anchors $\{w_i\}$. Formally, they define

$$\mathcal{P}_\beta = \left\{ \sum_i \alpha_i w_i \mid \sum_i \alpha_i = 1, \forall i : \alpha_i \geq -\beta \right\}, \quad (6)$$

where β is a positive, typically small, number defining the amount of dilation. Note that \mathcal{P}_β is a subspace of the generators \mathcal{W} latent space. The hyperparameter β is usually omitted from notation, and we instead denote the space as \mathcal{P} . With respect to \mathcal{P} , they choose to represent latent codes in Barycentric coordinates [Floater 2015], *i.e.*, using the convex coefficients $\{\alpha_i\}$. Optimization is thus technically performed on a vector of these coefficients – α . Changing back to standard coordinates is trivially done by $\sum_i \alpha_i w_i$.

Several measures are taken to ensure that the optimization process remains within the bounds of \mathcal{P}_β . First, the vector α is passed through a shifted softplus function:

$$\tilde{\alpha} = \frac{1}{s} \log(1 + e^{s(\alpha + \beta)}) - \beta, \quad (7)$$

where all operations are element-wise, and s is a “sharepness” hyperparameter we set to $s = 100$. This operation yields a new vector $\tilde{\alpha}$ whose minimal value is greater than $-\beta$.

Next, a regularization term is added to the optimization loss to encourage the sum of coefficients to be 1. Formally,

$$\mathcal{L}_{\text{sum}}(\tilde{\alpha}) = \left(\sum_i \tilde{\alpha}_i - 1 \right)^2. \quad (8)$$

Finally, the optimization result α^* is explicitly normalized to have a sum of 1.

B.2 Extended Latent Space, \mathcal{P}^+

First proposed by Abdal et al. [2019], an incredibly popular approach to increase StyleGAN’s expressivity is using an extended latent space \mathcal{W}^+ [Luo et al. 2020; Menon et al. 2020; Richardson et al. 2021]. Concisely, this latent space is composed by using a possibly different latent code in each layer of the generator. With its greater expressivity, it was also shown that \mathcal{W}^+ provides a less faithful prior. This has led previous works to regularize the extent to which it is exploited, *e.g.*, by encouraging latent code in different layers to still be similar under L_2 norm [Tov et al. 2021].

Nitzan et al. [2022] followed these ideas directly and imported them to \mathcal{P} . First, \mathcal{P} is extended to \mathcal{P}^+ across generator’s layers by allowing each layer to add an offset: $\alpha_\beta^+ = (\alpha_\beta + \Delta_0, \dots, \alpha_\beta + \Delta_N)$. Second, a regularization term is added to the optimization process and prevent severe deviation across layers. Formally,

$$\mathcal{L}_{\text{delta}}(\Delta) = \sum_i \|\Delta_i\|_2. \quad (9)$$

B.3 Final Optimization loss

The two regularization terms described in Eqs. (8) and (9) were jointly referred to in the main paper’s Eq. (5) as regularization terms assuring the optimization is constrained to the personalized latent space. The full optimization loss is thus given by

$$\mathcal{L}_{\text{full}} = \mathcal{L}_{\text{key}} + \lambda_{\text{mouth}} \mathcal{L}_{\text{mouth}} + \lambda_{\text{eyes}} \mathcal{L}_{\text{eyes}} + \lambda_{\text{delta}} \mathcal{L}_{\text{delta}} + \lambda_{\text{sum}} \mathcal{L}_{\text{sum}}. \quad (10)$$

ALGORITHM 1: Greedy algorithm to maximize subset’s diversity [Ravi et al. 1994].

Data: Set S , distance function d , subset size N .

Let s_i, s_j be the elements of set S who have the greatest distance d .

$T \leftarrow \{s_i, s_j\}$

while $|T| < N$ **do**

$s' \leftarrow \arg \max_{s \in S \setminus T} \min_{t \in T} d(s, t)$;

$T \leftarrow T \cup \{s'\}$;

end

Return T .

C ADDITIONAL TECHNICAL DETAILS

C.1 Self-Scan Frame selection

The formal description of the frame selection algorithm is provided in Algorithm 1.

C.2 Crops of the Mouth and Eyes

Our optimization’s pixel loss $\mathcal{L}_{\text{crop}}$ is calculated on crops of the mouth and eyes that are automatically extracted from the generated and driving frames. We next detail how these crops are obtained. We crop the minimal rectangles that bounds the keypoints from our subset for each region of interest – the outer parts of the lips and the irises. We then take center crops of the rectangles from the larger of the two rectangles, on each axis, to have the rectangles at the same size.

C.3 Implementation details

We next specify all hyperparameters. For the latent space, we use $\beta = 0.02$ in all experiments. The weights of the different loss terms $\lambda_{\text{crop}} = 1, \lambda_{\text{delta}} = 10, \lambda_{\text{sum}} = 10$. The additive Gaussian noise for the last frame result has $\sigma = 0.05$. The Gaussian low-pass filter on the produced latent codes has $\sigma = 2$. The number of self-scan frames in all experiments $N = 250$.

Training takes roughly 3.5 hours on a single V100, and optimization requires up to a minute for a single frame.